https://doi.org/10.5194/egusphere-2026-5464
Preprint. Discussion started: 29 September 2026

Particle-associated benzotriazole ultraviolet stabilizers exhibit atmospheric persistence against •OH heterogeneous oxidation

Kang Gao[1], Tianhong Zhang[1], Liuqing Zhao[2], Guangli Xiu[1], Xinke Wang[3], Lei Zhou[1*]

[1]State Environmental Protection Key Lab of Environmental Risk Assessment and Control on Chemical Processes, School of Resources and Environmental Engineering, East China University of Science and Technology, Shanghai 200237, China
[2]SCIEX Analytical Instrument Trading Co., Ltd, Shanghai 200000, China
[3]Shanghai Key Laboratory of Atmospheric Particle Pollution and Prevention (LAP3), National Observations and Research Station for Wetland Ecosystems of the Yangtze Estuary, Department of Environmental Science and Engineering, Fudan University, Shanghai 200438, China

Correspondence to: Lei Zhou (zhoulei@ecust.edu.cn)

Abstract. Benzotriazole ultraviolet stabilizers (BT-UVs) are ubiquitous in airborne particles due to continuous emissions from widespread usage in plastic and rubber, with several congeners recognized as Persistent Organic Pollutants (POPs) under the Stockholm Convention. While •OH-initiated heterogeneous oxidation is the primary atmospheric degradation pathway for particle-associated organics, the degradation kinetics and fate of particulate BT-UVs remain poorly constrained. Herein, an oxidation flow reactor (OFR) was utilized to systematically investigate the •OH-initiated heterogeneous oxidation processes of eight commonly used BT-UVs. The results revealed that the intrinsic second-order rate constants ranged from $(4.12 \pm 0.30) \times 10^{-13}$ to $(13.2 \pm 1.17) \times 10^{-13}$ cm^3 $molecules^{-1}$ s^{-1}, corresponding to atmospheric lifetimes exceeding one week and significant potential for long-range environmental transport (LRET). Furthermore, elevated ambient humidity enhanced their degradation rates by approximately 30%, whereas coexisting soluble iron exhibited a marginal effect. The oxidation proceeded mainly through alkyl-group and phenyl-ring reactions, yielding 30 tentatively identified transformation products (TPs), 24 of which were subsequently confirmed in ambient $PM_{2.5}$. These findings quantitatively confirm the high persistence of particulate BT-UVs and highlight the necessity of evaluating the environmental risks and human inhalation hazards of their secondary transformation products.

1 Introduction

Benzotriazole ultraviolet stabilizers (BT-UVs) are a class of additives capable of absorbing ultraviolet (UV) radiation and dissipating the absorbed energy as heat, thereby preventing photodegradation of materials (Parajulee et al., 2018; Chen et al., 2024; Zhao et al., 2024; Ling et al., 2025). Owing to this property, BT-UVs (Figure 1) have been extensively incorporated into industrial and consumer products such as plastics, textiles, and paints since the early 1960s (Castilloux et

https://doi.org/10.5194/egusphere-2026-5464
Preprint. Discussion started: 29 September 2026

al., 2022; Zhao et al., 2024; Ling et al., 2025). Through manufacturing emissions, volatilization, and mechanical abrasion of polymer materials (e.g., tire wear and plastic sports tracks), BT-UVs could be continuously released into the environment (Zhao et al., 2024). Due to their relatively low vapor pressures ($P < 1 \times 10^{-6}$ pa), BT-UVs emitted into the atmosphere partition predominantly into the particle phase (with a predicted fraction sorbed to airborne particles, $\Phi > 0.9$) rather than the gas phase (Huang et al., 2026). Consequently, they have become ubiquitous components of ambient aerosols, with measured concentrations reaching up to 30 ng m^{-3} in urban ambient air, depending on local emission intensity and ventilation conditions (Maceira et al., 2019; Zhao et al., 2024; Bai et al., 2025).

The inherent chemical stability that makes BT-UVs effective photo-protectors also raises profound concerns regarding their atmospheric persistence (Shunthirasingham et al., 2025). Recently, several commonly used BT-UVs have drawn intense regulatory scrutiny; for instance, UV-326, UV-327, and UV-328 have been listed as Substances of Very High Concern (SVHC) by the European Chemicals Agency (ECHA). Notably, UV-328 has been classified as a persistent organic pollutant (POP) under the Stockholm Convention. A critical criterion for this POP designation is the potential for long-range environmental transport (LRET) through the atmosphere. While their widespread occurrence and bioaccumulation in diverse environmental matrices (e.g., water, sediment, and biota) have been well documented (Nakata et al., 2009; Zhang et al., 2011; Lu et al., 2017; Zhang et al., 2021), the atmospheric compartment, which acts as the primary vector for their global distribution (Perala-Dewey and Hageman, 2024; Shunthirasingham et al., 2025), remains poorly characterized. Evaluating the LRET potential of particle-associated BT-UVs is currently hindered by a severe lack of kinetic data governing their atmospheric sinks.

In the atmosphere, the fate of particle-associated organic compounds is predominantly governed by heterogeneous oxidation initiated by hydroxyl radicals (•OH) (Laversin et al., 2016; Liu et al., 2021). Since the direct photolysis of BT-UVs on particles is highly inefficient with negligible degradation rates (Ling et al., 2025), •OH-induced multiphase oxidation serves as their primary degradation pathway. However, this multiphase process is highly complex and can be modulated by ambient conditions and particle chemical composition. For instance, ambient humidity governs aerosol liquid water content and particle viscosity, while coexisting transition metals (e.g., soluble iron) can trigger Fenton-like reactions; both factors can influence the uptake and diffusion of gas-phase •OH into the particle phase (Liu et al., 2019a). Furthermore, the atmospheric aging of BT-UVs yields a myriad of oxygenated transformation products (TPs). These TPs not only alter the physicochemical properties of the host aerosols but may also exhibit enhanced toxicity compared to their parent compounds, representing an unrecognized risk in atmospheric particulate matter (Li et al., 2009). Therefore, the lack of knowledge on •OH reactions, transformation products and thus persistence of particle-associated BT-UVs has severely constrained the current understanding of them in the atmospheric environment.

To address these gaps, this study systematically investigated the •OH-initiated heterogeneous oxidation chemistry of eight commonly used BT-UVs (including UV-P, UV-234, UV-326, UV-327, UV-328, UV-329, UV-360 and UV-928) coated onto simulated atmospheric particles. Specifically, our objectives were to: (1) determine the heterogeneous oxidation kinetics of particle-associated BT-UVs by gas-phase •OH; (2) quantitatively evaluate their atmospheric persistence and

https://doi.org/10.5194/egusphere-2026-5464
Preprint. Discussion started: 29 September 2026

LRET potential; (3) evaluate the impact of RH and coexisting soluble iron on their degradation kinetics; (4) identify the •OH heterogeneous oxidation pathways and structurally characterize the resulting TPs, followed by their screening in ambient $PM_{2.5}$; and (5) conduct a preliminary toxicity assessment of the parent BT-UVs and their atmospheric TPs. By linking fundamental multiphase kinetics with field observations, this study would provide quantitative constraints on the atmospheric fate of BT-UVs and fundamental data for future environmental risk assessments.

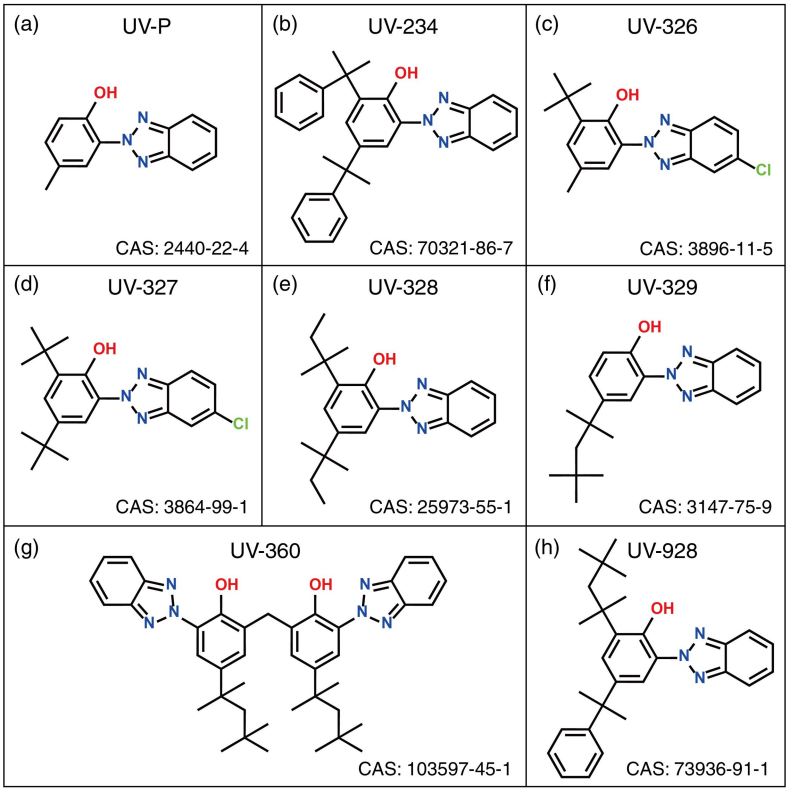

Figure 1. Chemical structures of target BT-UVs.

2 Materials and Methods

2.1 Chemicals and Reagents

Reference standards of eight target BT-UVs, including UV-P, UV-234, UV-326, UV-327, UV-328, UV-329, UV-360 and UV-928 were purchased from Macklin Biochemical Co., Ltd. (Shanghai, China) with purities higher than 99%. Detailed information regarding these compounds is provided in Table S1 in the Supplement. Ammonium sulfate, ferrous sulfate heptahydrate, and ammonium acetate were also obtained from the same supplier (purities > 98%). In this study, $(NH_4)_2SO_4$ (AS) particles were used as a proxy for preexisting ambient aerosols, serving as inert seeds for the heterogeneous condensation. Additionally, $FeSO_4$ (FS) particles were used to examine the impacts of coexisting soluble iron on the

https://doi.org/10.5194/egusphere-2026-5464
Preprint. Discussion started: 29 September 2026

degradation kinetics of BT-UVs. Analytical grade hexane, acetone, and methanol, along with HPLC-grade methanol and formic acid were purchased from Merck KGaA (Darmstadt, Germany). Ultra-pure water was prepared using the Milli-Q system (Bedford, MA, United States). Pure N_2, O_2, and a gas mixture containing 5 ppm SO_2 in a N_2 matrix were purchased from Air Liquide (Shanghai, China).

2.2 Coating Particles

Seed aerosol particles were generated by atomizing a 5.3 mM $(NH_4)_2SO_4$ (or $FeSO_4$, depending on the experimental objectives) aqueous solution by an aerosol generator (TSI, Model 3079A) with a carrier flow rate of 1.5 L min^{-1}. A diffusion dryer (TSI, Model 3062) was employed to produce dry, polydisperse particles with a geometric mean diameter of approximately 50 nm, as characterized by a scanning mobility particle sizer (TSI, Model 3938). Pure BT-UVs were heated to 373-403 K in a heated chamber installed downstream of the diffusion dryer. Consistent with heterogeneous condensation principles, organic vapor could rapidly condense onto cold particles. These core-shell particles displayed organic–inorganic phase separation, where the BT-UVs constituted an outer shell surrounding the inorganic core (Reid et al., 2011; Song et al., 2013; Wang et al., 2024). The coating thickness of each individual BT-UV coating on seed particle surface was determined to be approximately 10 nm (Figures S2 and S3). Additionally, an activated carbon trap was used to remove any uncondensed organic vapor prior to injecting the aerosols into the oxidation flow reactor (OFR).

2.3 Heterogeneous Oxidation

Heterogeneous oxidation experiments for particle-associated BT-UVs were conducted in a customized OFR (Figure S1), which was operated under OFR-185 mode (Peng and Jimenez, 2020). N_2 and O_2 were fully mixed with coated particles prior to injection into the OFR, with a total flow rate of 2.5 L min^{-1}. The number concentration of coated particles within the OFR was stable at 1.4×10^6 particles cm^{-3}, and the corresponding residence time was calculated to be approximately 100 s. Upon UV irradiation in the OFR (light intensity of 2.0 mW cm^{-2}), gas-phase $^{\bullet}OH$ could be mainly generated via two pathways, photolysis of H_2O at 185 nm and photolysis of O_3 at 254 nm ($O(^1D)$ reacts with H_2O). Temperature and relative humidity (RH) in the OFR were monitored using an internal sensor (Huakong, Model HSTL-F107). During the experiment, the temperature in the OFR was maintained at 298 K by circulating water in the outer jacket, while the RH was regulated by bubbling N_2 through an aqueous solution.

2.4 $^{\bullet}OH$ Exposure

To achieve reliable quantification of $^{\bullet}OH$ exposure ($^{\bullet}OH_{exp}$) for particle-associated BT-UVs in the OFR, $^{\bullet}OH_{exp}$ (molecules cm^{-3} s) was determined by monitoring the decay of SO_2 in offline calibrations (Li et al., 2015; Peng et al., 2018), as described by Eq (1):

$$^{\bullet}OH_{exp} = -\frac{1}{k_{SO_2}} \ln \frac{[SO_2]_t}{[SO_2]_0} \quad (1)$$

https://doi.org/10.5194/egusphere-2026-5464
Preprint. Discussion started: 29 September 2026

where k_{SO_2} was the second-order rate constant for the reaction of SO_2 with $^{\bullet}OH$ at 298 K, with a literature value of 9.5×10^{-13} cm^3 $molecules^{-1}$ s^{-1} (Li et al., 2015); $[SO_2]_0$ was the initial SO_2 concentration at the OFR inlet; $[SO_2]_t$ represented the final concentration at the OFR outlet. The decay of SO_2 in offline calibrations were determined by a SO_2 analyzer (Thermo Scientific, Model 43i). The determined $^{\bullet}OH_{exp}$ in the OFR ranged from 3.5×10^{11} to 6.6×10^{11} molecules cm^{-3} s at 25% RH and from 4.1×10^{11} to 8.9×10^{11} molecules cm^{-3} s at 50% RH (Table S2).

2.5 Impacts of Photolysis and Ozonolysis

Potential loss of each individual BT-UV induced by photolysis and ozonolysis in the OFR was assessed through supplementary control experiments. To quantify photolysis loss, BT- UVs film with a thickness of 10 nm was prepared, with detailed procedures provided in Text S2 in the Supplement. The coated films were irradiated with UV lamp for 100 s and subsequently extracted ultrasonically with acetone. For the ozonolysis experiments, O_3 was generated via the photolysis of O_2 at 185 nm in an ozone generator (Tonglin, Model UV-PRO), and mixed with coated particles prior to injection into the OFR. The concentration of O_3 in the OFR was determined to be 15 ppm (representing the maximum concentration during the heterogeneous oxidation experiments), yielding an O_3 exposure of 3.7×10^{16} molecules cm^{-3} s over a 100 s residence time.

2.6 Air Sampling

To screen the TPs of BT-UVs in ambient $PM_{2.5}$, a total of 18 ambient $PM_{2.5}$ samples were collected in Shanghai, China (31°N, 121°E), during December 19 to 27, 2025 using a high-volume active air sampler (Tianhong, Model TH-1000). Prior to sampling, quartz filters were pre-baked in a muffle furnace at 500 °C for 4 h to eliminate background organic contaminants. During each sampling event, $PM_{2.5}$ was collected on a quartz filter for 12 h at a flow rate of 1000 L min^{-1}, corresponding to a total sampled air volume of 720 m^3. After collection, all filters were wrapped in aluminium foil and stored at −20 °C until further analysis.

2.7 Sample Extraction

In this study, $PM_{2.5}$ samples were extracted with an acetone–hexane mixture (1:1, v/v). The extracts were ultrasonicated for 1 h in an ice-water bath under dark conditions, followed by 5 min of centrifugation at 4000 rpm to collect the supernatant. The supernatant was then evaporated to dryness under a gentle nitrogen stream and reconstituted in 1 mL of methanol. The resulting solution was filtered through a 0.22 μm polytetrafluoroethylene (PTFE) membrane and stored at −20 °C prior to instrumental analysis.

2.8 Instrumental Analysis

Quantification of the target BT-UVs was performed using an ultra-performance liquid chromatograph (ExionLC™, SCIEX) coupled to a quadrupole mass spectrometer (QTRAP® 6500+, SCIEX) operated in multiple reaction monitoring

https://doi.org/10.5194/egusphere-2026-5464
Preprint. Discussion started: 29 September 2026

(MRM) mode. Chromatographic separation was achieved on an ACQUITY Premier BEH C18 column (1.7 μm, 100 × 2.1 mm), with an injection volume of 3.0 μL. Suspect screening of oxidation products was performed using an ultra-performance liquid chromatograph (ExionLC™, SCIEX) coupled to a time-of-flight mass spectrometer (X500B QTOF, SCIEX) in the information-dependent acquisition (IDA) mode. The mass defect filter was enabled during HRMS acquisition to improve the signal quality of MS^2 spectra. Chromatographic separation was achieved on a Kinetex® C18 column (2.6 μm, 100 × 2.1 mm), with an injection volume of 5.0 μL. Details of the gradient elution program and instrument parameters are provided in Texts S3 and S4 in the Supplement.

2.9 Kinetics and Lifetimes

The observed second-order rate constants (k_{obs}, cm^3 $molecule^{-1}$ s^{-1}) for the reaction of particle-associated BT-UVs with gas-phase ·OH were fitted using the empirical equation (Pflieger et al., 2013; Chan et al., 2014):

$$\ln\frac{C_t}{C_0} = -k_{obs}[OH]t \quad (2)$$

where C_0 was the initial concentration of BT-UVs; C_t was the concentration of BT-UVs after ·OH oxidation; [OH] represented the steady-state (SS) concentration of ·OH; and t was the residence time.

The ·OH reactive uptake coefficient (γ_{obs}) was calculated using the core–shell diffusion-reaction expression reported in the literature (Smith et al., 2009):

$$\gamma_{obs} = \frac{4k_{obs}\rho(r_p^3 - r_c^3)N_A}{3r_p^2\bar{c}M_w} \quad (3)$$

where ρ was the density of BT-UVs; r_p was the particles radius; r_c represented the radius of the core; N_A was the Avogadro's number; $\bar{c}$ represented the mean speed of gas-phase ·OH; and M_w was the molecular weight of BT-UVs.

To account for mass-transfer limitations caused by the gas-phase diffusion of ·OH, the measured k_{obs} values were corrected to obtain the intrinsic experimental second-order rate constants (k_{exp}, cm^3 $molecule^{-1}$ s^{-1}) of particle-associated BT-UVs, using the Fuchs-Sutugin transitional regime correction framework (Fuks and Sutugin, 1970; Worsnop et al., 2002):

$$Kn = \frac{\lambda}{r_p} \quad (4)$$

$$\frac{1}{\Gamma} = \frac{0.75 + 0.238Kn}{Kn(1+Kn)} \quad (5)$$

$$\frac{1}{\gamma_{obs}} = \frac{1}{\Gamma} + \frac{1}{\gamma_{exp}} \quad (6)$$

$$\frac{k_{exp}}{k_{obs}} = \frac{\Gamma}{\Gamma - \gamma_{obs}} \quad (7)$$

where Kn was the Knudsen number; λ represented the gas-phase mean free path of ·OH; Γ was the diffusion-limited uptake coefficient.

The atmospheric lifetimes (τ) and half-lives ($t_{1/2}$) for particle-associated BT-UVs in the troposphere were calculated using the Eq (8) and Eq (9) (Cousins et al., 2019):

https://doi.org/10.5194/egusphere-2026-5464
Preprint. Discussion started: 29 September 2026

$$\tau = \frac{1}{k_{exp}[OH]_{GM}} \quad (8)$$

$$t_{1/2} = \frac{0.693}{k_{exp}[OH]_{GM}} \quad (9)$$

where $[OH]_{GM}$ was the global mean concentration of gas-phase ·OH, ranging from 6.5×10^5 to 1.6×10^6 molecules cm^{-3} (Lawrence et al., 2001).

2.10 AOPWIN Prediction.

To clarify the disparities between ·OH-initiated oxidation of BT-UVs in the particle phase and in the gas phase, the US EPA-developed Atmospheric Oxidation Program (AOPWIN) model was utilized to predict second-order rate constants (k_{AOPWIN} , cm^3 $molecule^{-1}$ s^{-1}) for the reaction of gas-phase BT-UVs with ·OH. This model employs a structure–activity relationship (SAR) approach, wherein the k_{AOPWIN} values are estimated by summing empirically derived reactivity contributions from individual molecular fragments and functional groups identified from the input SMILES structure (Meylan and Howard, 1993; Atkinson, 2002).

2.11 Long-range Environmental Transport (LRET) Potential

The LRET of BT-UVs was assessed using the OECD Overall Persistence and Long-Range Transport Potential Screening Tool (Wegmann et al., 2009). The screening tool predicted the overall environmental persistence (P_{OV}), characteristic travel distance (CTD), and remotely transfer efficiency (φ2) of BT-UVs based on their partition coefficients (e.g., log K_{ow} and log K_{oa}) and $t_{1/2}$. The $t_{1/2}$ values of BT-UVs in air were adopted from measured values determined in this study, while those in water and soil were predicted using EPI Suite™ (Mackay et al., 1996). For benchmarking, the calculated metrics were directly compared with those of reference persistent organic pollutants (POPs).

2.12 Toxicity Assessment

Predicted no-effect concentrations (PNEC) were employed to preliminarily assess the ecotoxicity of the target environmental contaminants and their TPs (Yang et al., 2026). PNEC values was defined as the ratio of the acute median lethal concentration (LC_{50}) and an appropriate assessment factor (AF) (Van Leeuwen, 1996). For systemic toxicity evaluation, human oral exposure can be considered equivalent to inhalation exposure when local respiratory tract effects are negligible (U.S. EPA, 1994). In the absence of available experimental toxicity data, acute oral rat LC_{50} values were predicted with the U.S. EPA TEST model for subsequent PNEC derivation (Ccte, 2022). Considering the structural uncertainty of TPs, a conservative assessment strategy was adopted, with the AF set to 1000 to avoid underestimating their toxic potential (Yang et al., 2026). Toxicity variation coefficient (TVC) was calculated to quantify the toxicity variation between TPs and their parent compounds:

$$TVC = \frac{PNEC_P}{PNEC_{TPs}} - 1 \quad (10)$$

https://doi.org/10.5194/egusphere-2026-5464
Preprint. Discussion started: 29 September 2026

where $PNEC_P$ and $PNEC_{TPs}$ were the PNEC values of parent compounds and their corresponding TPs, respectively.

3 Results and Discussion

3.1 Oxidation Kinetics of Particle-associated BT-UVs

To eliminate the interference of background components, the inert $(NH_4)_2SO_4$ particles were used as proxies for preexisting ambient aerosols (Liu et al., 2021), and the pre-synthesized core shell particles were used to preliminarily explore the heterogeneous oxidation kinetics for BT-UVs initiated by gas-phase •OH. Prior to determining the •OH oxidation rate constants, potential loss of the target BT-UVs via direct photolysis and ozonolysis in the OFR were evaluated, as these processes could result in kinetic overestimations (Liu et al., 2021). These control experiments revealed no evident photolysis or ozonolysis (both less than 5%), which could be attributed to the short residence of the coated particles and relatively low O_3 exposure. Additionally, the evaporation losses of BT-UVs in OFR were estimated to be less than 0.2% based on the empirical equations for Fick's first law of diffusion (Jacobson, 2005), suggesting a minor effect on the •OH heterogeneous oxidation kinetics.

The reaction kinetics between particle-associated BT-UVs and gas-phase •OH were initially investigated at 298 K under 25% RH (Figure 2a-h). As seen, derived second-order rate constants (k_{obs}) ranged from 10^{-13} to 10^{-12} cm^3 $molecule^{-1}$ s^{-1}, consistent with typical semi-volatile organic compounds (SVOCs) reaction in the solid phase. From an atmospheric modeling perspective, the derived k_{obs} can be constrained by the diffusion rate of •OH from the gas phase to the particle surface (Davidovcits et al., 2006). In general, gas-phase diffusion did not limit the uptake of •OH by BT-UVs on nano-sized aerosol particles, yet corrections were required. Accordingly, to assess whether gas-phase diffusion limited the present measurements, the k_{obs} values were recalculated using the empirical equations (Fuks and Sutugin, 1970; Worsnop et al., 2002). Consequently, the resulting intrinsic experimental second-order rate constants (k_{exp}) ranged from $(4.12 \pm 0.30) \times 10^{-13}$ to $(13.2 \pm 1.17) \times 10^{-13}$ cm^3 $molecules^{-1}$ s^{-1}, with corresponding •OH reactive uptake coefficients (γ_{exp}) between $(7.41 \pm 0.53) \times 10^{-2}$ to $(7.01 \pm 0.63) \times 10^{-2}$ (Table S4).

Specifically, the k_{exp} values followed an increasing order, with UV-P < UV-326 < UV-327 < UV-328 < UV-928 < UV-234 < UV-329 < UV-360 (Figure 2i). This kinetic variance is highly dependent on substituent effects. For instance, alkyl groups with abstractable C-H bonds (e.g., tert-butyl and tert-amyl in UV-360) were proposed to provide additional active sites for •OH abstraction (Huang et al., 2026). Conversely, chlorine substituents (e.g., UV-326) could decrease the π electron density of the aromatic ring, thus rendering it less susceptible to electrophilic attack by •OH

In the absence of any reported •OH heterogeneous oxidation rate constants for particle-associated BT-UVs, their reactivity toward •OH could only be inferred by comparison with other organic contaminants for which kinetic data are available. Overall, the k_{exp} values of particle-associated BT-UVs are slightly lower than those for liquid crystal monomers (LCMs) (Liu et al., 2020), but higher than those of organophosphate flame retardants (OPFRs) and terbuthylazine (Liu et al., 2014; Han et al., 2021), indicating moderate •OH reactivity in the atmospheric particle phase.

https://doi.org/10.5194/egusphere-2026-5464
Preprint. Discussion started: 29 September 2026

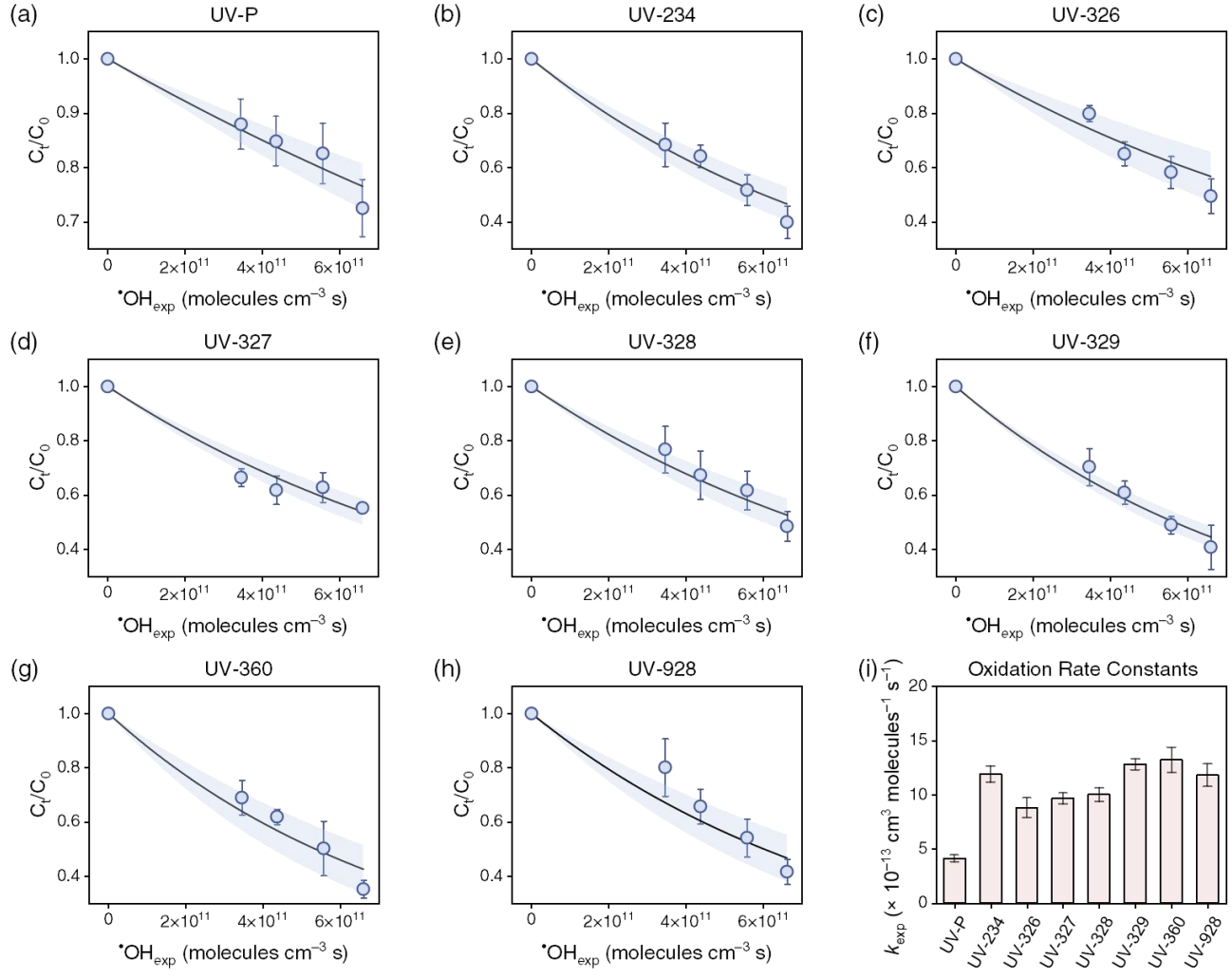

230 **Figure 2. Heterogeneous oxidation kinetics curves for eight target BT-UVs (a-h), and the derived intrinsic second-order oxidation rate constants (k_{exp}) (i) for particle-associated BT-UVs.**

3.2 Atmospheric Persistence and LRET Potential

Numerous studies have verified that BT-UVs preferentially partition into atmospheric particles, with only a minor proportion remaining in the gas phase (Zhao et al., 2024; Shunthirasingham et al., 2025; Huang et al., 2026). Consequently,
235 their atmospheric persistence is generally governed by the particle-phase lifetimes. However, due to the scarcity of available data on the particle-phase persistence of BT-UVs, existing global regulatory frameworks rely heavily on gas-phase •OH oxidation parameters, which might result in biased risk assessments. To quantify the persistence disparities, AOPWIN model was initially employed to estimate the second-order rate constants (k_{AOPWIN}) for the reaction of gas-phase BT-UVs with •OH (Meylan and Howard, 1993; Atkinson, 2002). As seen in Figure 3a, the predicted k_{AOPWIN} values ranged from 1.32×10^{-11} to

https://doi.org/10.5194/egusphere-2026-5464
Preprint. Discussion started: 29 September 2026

240 3.32 × 10^{-11} cm^3 $molecules^{-1}$ s^{-1}, which were at least one order of magnitude higher than k_{exp} (Figure 3b). This kinetic disparity aligned with findings reported for OPFRs (Liu et al., 2019b), indicating that ·OH oxidation rates of SVOCs were universally inhibited in the particle phase. This significant inhibition could be primarily attributed to the slow diffusion of ·OH in the particle-phase reaction system (Zhou et al., 2013; Huang et al., 2026).

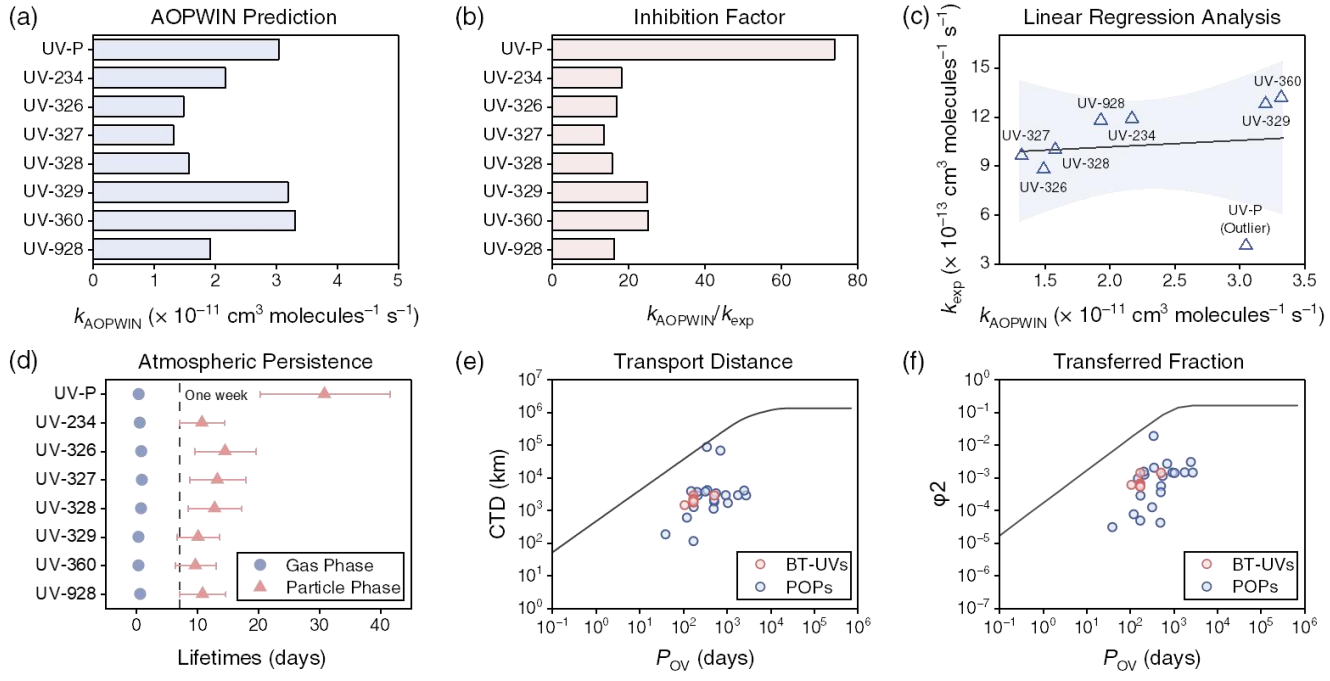

245 **Figure 3. AOPWIN-predicted second-order oxidation rate constants (k_{AOPWIN}) (a), inhibition factors (b), linear regression analysis (c) and atmospheric persistence (d) of BT-UVs in the particle and gas phases, and their transport distance (CTD) (e) and transferred fraction (φ2) (f) in the environment.**

Additionally, a linear regression analysis was performed between k_{exp} and k_{AOPWIN} (Figure 3c). Interestingly, most BT-UVs exhibited an approximate linear correlation; however, UV-P deviated markedly from the regression line, acting as a 250 significant outlier. Although the k_{exp} of UV-P was substantially lower than those of the other BT-UVs, its ·OH uptake coefficient (7.41 × 10^{-2}) was comparable to the others (ranging from 7.01 × 10^{-2} to 13.5 × 10^{-2}). A plausible explanation was the smaller molecular size of UV-P allowed it to form a highly dense coating on the particle surface, which sterically restricts the inward diffusion of ·OH, resulting in a significantly lower apparent oxidation rate. This substantial phase-dependent disparity in ·OH oxidation rates critically impacts their atmospheric lifetimes (τ, Figure 3d). The estimated τ for 255 BT-UVs ranged from 9.7 ± 3.3 to 31 ± 11 days in particle phase, compared to merely 0.38 ± 0.13 to 0.95 ± 0.33 days in gas phase (Table S5). Even when assessment models adopt relatively high global ·OH concentration parameters, the τ values of all particle-associated BT-UVs exceed five days, with most surpassing a full week.

https://doi.org/10.5194/egusphere-2026-5464
Preprint. Discussion started: 29 September 2026

As can be expected, this prolonged resistance to degradation directly facilitated their LRET potential. To contextualize this LRET potential against global regulatory criteria, the overall environmental persistence (P_{OV}) and transport metrics of BT-UVs were simulated using the OECD-endorsed screening tool and benchmarked against existing POPs (Tables S6 and S7). As shown in Figure 3e-f, the modeling yielded P_{OV} values ranged from 1.08×10^2 to 5.19×10^2 days, with corresponding CTD spanning 1.43×10^3 to 2.86×10^3 km, and φ2 of 5.23×10^{-4} to 1.41×10^{-3}. These metrics were highly comparable to those of established POPs regulated under the Stockholm Convention, providing robust mechanistic evidence that BT-UVs possessed substantial LRET capabilities. Furthermore, these modeling constraints were strongly corroborated by recent field monitoring data, which documented the successful detection of UV-P in remote atmospheric environments (Shunthirasingham, 2025).

3.3 Impact of Relative Humidity and Coexisting Soluble Iron

In the atmosphere, environmental humidity generally governed the water content and deliquescence properties of aerosol particles, thereby influencing the mass transport and diffusion of gas-phase •OH within particles (Slade and Knopf, 2014). In addition, ubiquitous transition metals like iron, with concentrations up to 5.2 μg m^{-3}, and can trigger Fenton-like reactions (He et al., 2001). Previous studies have confirmed that Fenton-like reactions initiated by the unique redox activity of Fe(II) modulated the multiphase oxidation behaviour of SVOCs on aerosol particles (Daumit et al., 2016; Liu et al., 2019a). Given that the effects of environmental conditions and particle constituents on the atmospheric persistence of particle-associated BT-UVs remain unclear, the impacts of RH and redox-active Fe(II) on their degradation kinetics were systematically investigated in this study. To this end, gas-phase •OH diffusion corrections were applied to obtain the k_{exp} values of BT-UVs coated onto AS particles as well as FS particles at 25% and 50% RH, and their corresponding atmospheric lifetimes were calculated (Tables S8 and S9).

As shown in Figure 4a, increasing RH from 25% to 50% significantly enhanced the •OH oxidation rate of most BT-UVs, resulting in an average increase of ~30% in their corresponding k_{exp}. This promotion can be attributed to the elevated particle water content and reduced matrix viscosity, which facilitated the diffusion of •OH within the particle phase (Slade and Knopf, 2014; Liu et al., 2019a). Unlike the pronounced effects of RH, the presence of Fe(II) in the aerosol particles did not significantly enhance the •OH oxidation rate at either 25% or 50% RH, yielding only a marginal average increase of ~10% in k_{exp}. Consequently, these results indicated that potential Fenton-derived •OH played a minor role in the heterogeneous oxidation processes under the moderate humidity conditions examined in this study. However, a previous study has demonstrated that at higher RH levels (e.g., 68%), the deliquescence of FS particles may significantly promote the out-shell oxidation of SVOCs (e.g., up to 53%) (Liu et al., 2019a). This discrepancy can be rationalized by phase transition threshold effects, at relatively low-to-moderate RH (25-50 %), water uptake was substantially hindered by the hydrophobic BT-UV outer shell, which suppressing the hygroscopicity of the internal FS core and thereby inhibiting the initiation of Fenton reactions. Only when the RH exceeded the specific deliquescence threshold does the core undergo complete phase transition to activate Fenton-driven chemistry.

https://doi.org/10.5194/egusphere-2026-5464
Preprint. Discussion started: 29 September 2026

As illustrated in Figure 4b, at 50% RH, estimated τ (Figure 4b) for BT-UVs ranged from 8.4 ± 2.9 to 16 ± 5.6 days on AS particles, and from 7.6 ± 2.6 to 16 ± 5.5 days on FS particles. These values were consistently shorter than those observed at 25 % RH, which spanned from 9.7 ± 3.3 to 31 ± 11 days on AS and from 9.3 ± 3.2 to 23 ± 7.9 days on FS particles. Notably, under actual atmospheric conditions, wet deposition and precipitation scavenging can further accelerate the removal of these particle-associated contaminants from the atmosphere (Awonaike et al., 2021).

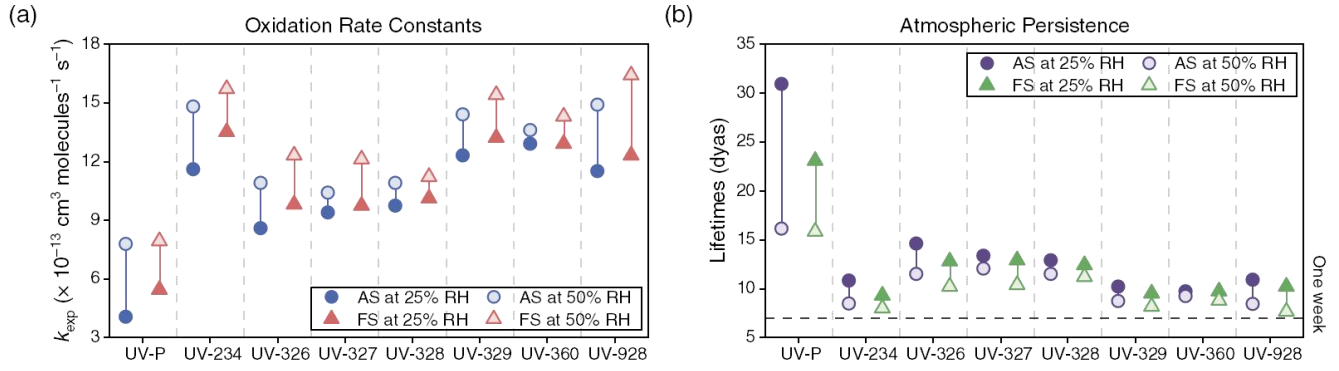

Figure 4. Second-order oxidation rate constants (k_{exp}) of particle-associated BT-UVs at different conditions (a), and their corresponding lifetimes (b).

3.4 Oxidation Pathway and Products of Particle-associated BT-UVs

Following the modified suspect screening workflow reported previously (Yang et al., 2026), a total of 30 TPs of BT-UVs were tentatively identified via high-resolution mass spectrometry (HRMS) analysis, with more details are provided in Table S10 in the Supplement. While the unambiguous structural resolution of certain isomers remains constrained by collision-activated dissociation (CAD) limitations and low environmental extraction concentrations (Huang et al., 2026), these robust qualitative findings still enabled a reliable preliminary deduction of the •OH multiphase oxidation pathways. Generally, the degradation could be broadly classified into two categories: (I) alkyl group oxidation and (II) phenyl ring oxidation. In this section, UV- 328 and UV-234 was chosen as a representative case for further discussion (Figure 5).

https://doi.org/10.5194/egusphere-2026-5464
Preprint. Discussion started: 29 September 2026

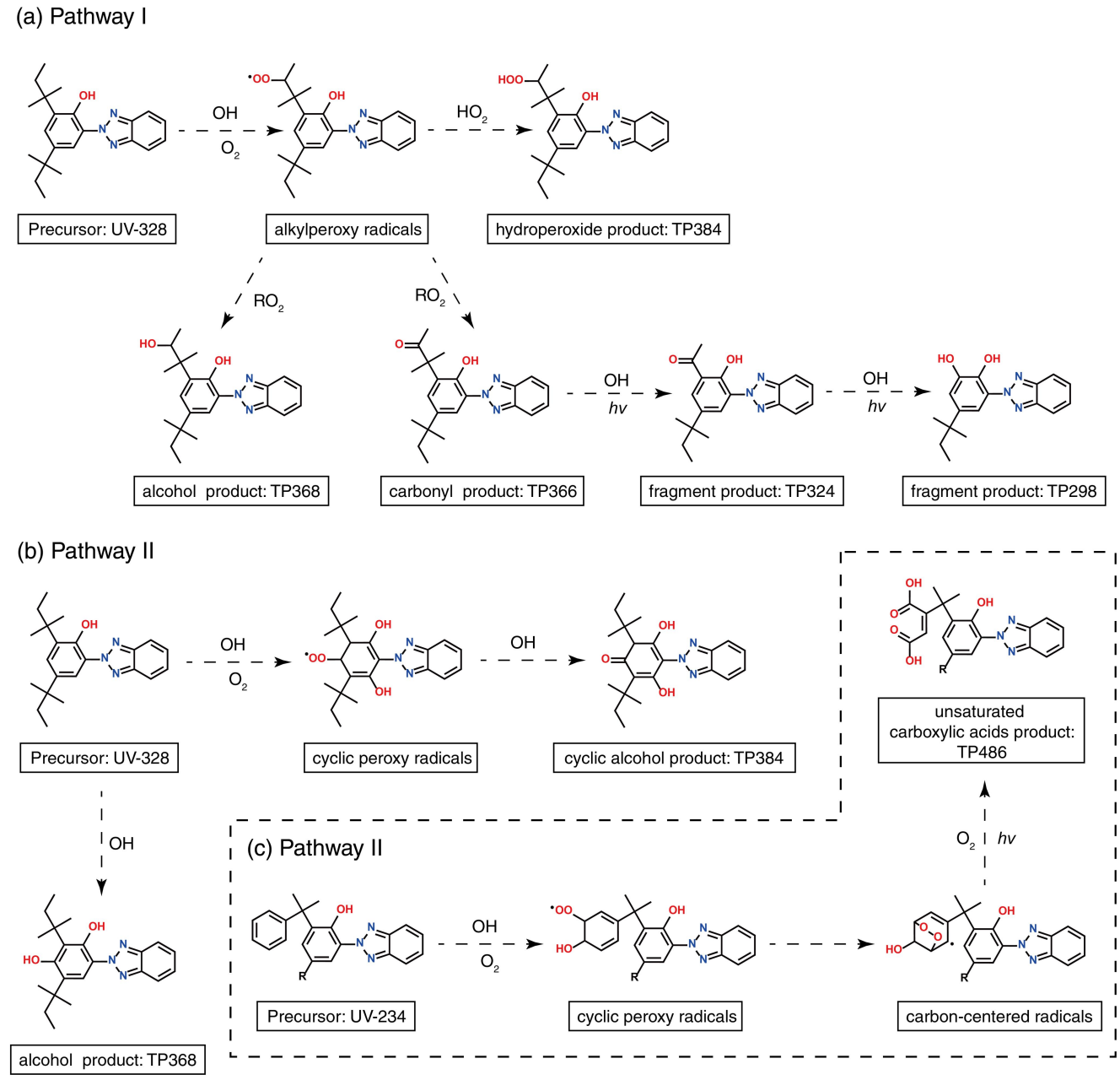

Figure 5. Proposed ·OH heterogeneous oxidation pathways for UV-328 (a-b) and UV-234 (c).

Specifically, in pathway I (Figure 5a), the reaction was initiated by ·OH-mediated H-abstraction from the alkyl group of UV-328, yielding alkylperoxy radicals. These radicals subsequently reacted with HO_2· to generate a hydroperoxide product (TP384, R.T. = 5.0 min). Alternatively, via the classical Russell mechanism (Russell, 1957; Miyamoto et al., 2003), the

https://doi.org/10.5194/egusphere-2026-5464
Preprint. Discussion started: 29 September 2026

bimolecular reaction of alkylperoxy radicals with $RO_2^{\bullet}$ to produce an alcohol (TP368, R.T. = 5.0 min) and a carbonyl (TP366, R.T. = 4.9 min). Such bimolecular path has recently been reported for H-abstraction reactions of UV-328 in nm-thick films (Huang et al., 2026). Upon continued $^{\bullet}OH$ oxidation, these intermediates could further undergo sequential decomposition, giving rise to short-chain fragment (TP324(1), R.T. = 4.8 min, and TP298, R.T. = 4.6 min), a process analogous to the previously proposed photooxidation mechanism for OPFRs (Liu et al., 2019b). In pathway II (Figure 5b), $^{\bullet}OH$ can directly add to the phenyl ring of UV-328 to form a phenolic product isomeric to TP368 (R.T. = 4.6 min). Additionally, $^{\bullet}OH$ attack on the phenyl ring could also produce cyclic peroxy radicals (Birdsall et al., 2010), which further reacted with $^{\bullet}OH$ to afford a cyclic alcohol product isomeric to TP384 (R.T. = 4.6 min). Moreover, cyclic peroxy radicals could experience O_2-induced isomerization to carbon-centered radicals (Figure 5c), triggering ring-opening reactions that yield unsaturated dicarbonyls and carboxylic acids products (e.g., TP486). Interestingly, such extensive ring-opening was exclusively observed for BT-UVs bearing additional independent phenyl moieties (e.g., UV-234). In contrast, the core benzotriazole structure exhibited remarkable chemical stability, firmly resisting ring-cleavage under the current $^{\bullet}OH$ exposure conditions.

3.5 Occurrence and Toxicity of BT-UVs and TPs in Ambient $PM_{2.5}$

To investigate the atmospheric occurrence of BT-UVs and their tentative TPs, target screening was further conducted in $PM_{2.5}$ samples collected in typical megacity (Shanghai, China). Briefly, all investigated BT-UVs were successfully detected in the $PM_{2.5}$ samples, with their total concentration ranging from 46.6 to 235 pg m^{-3} during the collection period (Table S11), which was comparable to those quantified in PM samples from Toronto (Shunthirasingham et al., 2025). The relative abundances of BT-UVs (Figure 6a) in the $PM_{2.5}$ samples followed an increasing in the order: UV-928 < UV-327 < UV-328 < UV-360 < UV-P < UV-234 < UV-329 < UV-326. Notably, UV-234, UV-326, and UV-329 together accounted for more than 70% of the total BT-UV burden, establishing them as the predominant BT-UV components in Shanghai's $PM_{2.5}$. Additionally, tentative TPs were also screened in these samples and semi-quantified based on chromatographic peak areas. Of the 30 candidate TPs, 24 of them were successfully detected in the $PM_{2.5}$ samples, whereas the remaining 6 TPs were below the detection limit. The quantification analysis results (Figure 6b) demonstrated that the concentrations of the TPs derived from specific BT-UVs varied markedly in the $PM_{2.5}$ samples, for instance, TP298 emerged as the predominant transformation product of UV-328.

Given the widespread occurrence of BT-UVs and their TPs in urban aerosols, it is essential to evaluate their potential health risks. Therefore, PNEC values for both parent compounds and TPs were derived from acute oral toxicity predictions combined with established assessment factors (Van Leeuwen, 1996; Ccte, 2022; Yang et al., 2026). For TPs with multiple possible isomers, the highest PNEC value was conservatively adopted to avoid underestimating ecological or health hazards. As shown in Figure 6c, the PNEC values for BT-UVs and their TPs ranged from 1.4×10^2 to 3.0×10^3 μg kg^{-1} (Table S12). Specifically, UV-360 exhibited a lower PNEC than the other BT-UVs, indicating higher potential toxicity, despite its relatively low abundance in $PM_{2.5}$ (<10%). In contrast, UV-329, with a relative abundance of 28%, showed the lowest

https://doi.org/10.5194/egusphere-2026-5464
Preprint. Discussion started: 29 September 2026

toxicity among all investigated compounds. Apart from the intrinsic toxicity of BT-UVs, highly oxygenated products exhibited amplified toxicological profiles, a phenomenon well-documented for other SVOC classes (Li et al., 2009; Antiñolo et al., 2015). According to the prediction results, a total of 22 TPs were predicted to be more toxic than their parent compounds, with toxicity variation coefficient (TVC) values ranging from 0.01 to 4.19, while only 8 TPs showed reduced toxicity, with TVC values between –0.02 and –0.84. Although a substantial fraction of TPs exhibited elevated intrinsic toxicity, their relatively low ambient abundances in $PM_{2.5}$ suggested that the actual toxicity enhancement in the atmosphere might be limited.

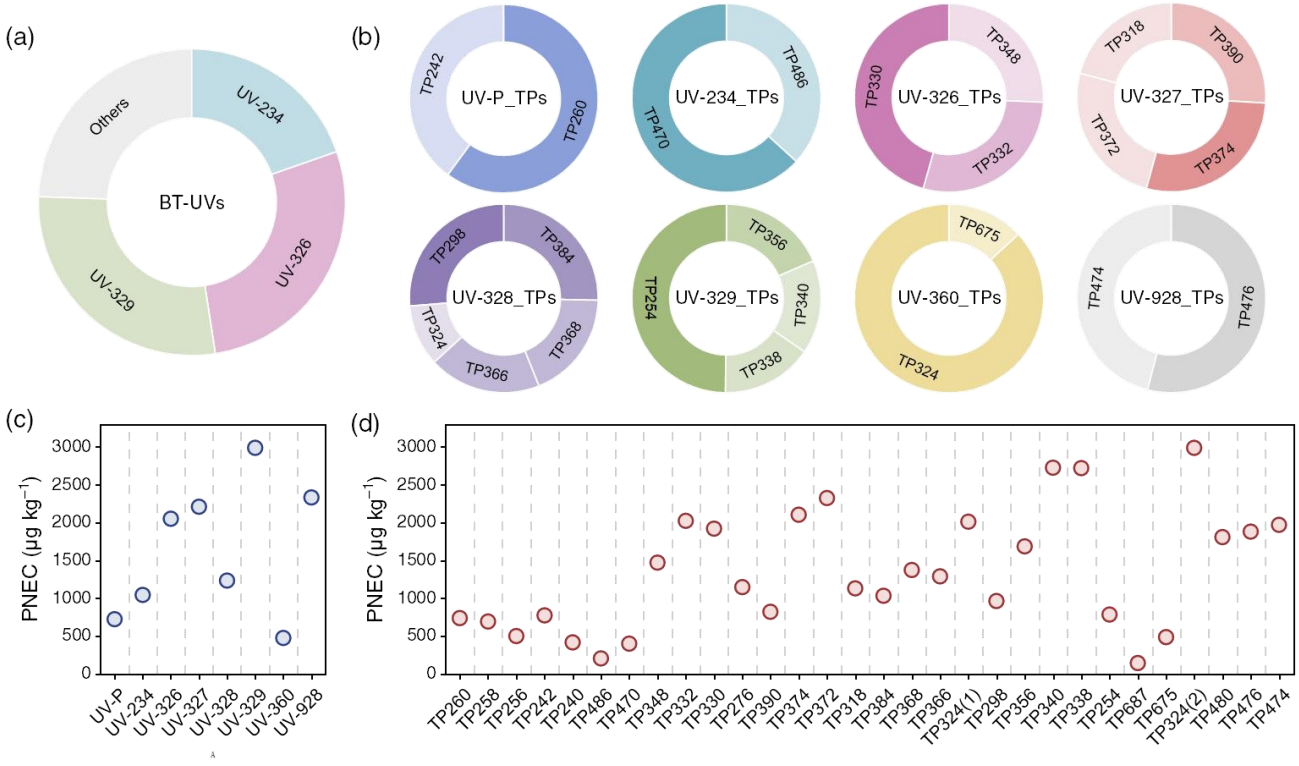

Figure 6. Relative abundance (a-b) of BT-UVs and TPs in Shanghai's $PM_{2.5}$, and their predicted no-effect concentrations (PNEC) (c-d).

4 Conclusion

This study systematically investigated the multiphase $^{\bullet}OH$-initiated heterogeneous oxidation kinetics and transformation pathways of eight particle-associated BT-UVs, directly linking laboratory kinetics parameters to global atmospheric persistence. Under idealized atmospheric conditions (298 K, 25% RH), the derived intrinsic second-order rate constants ranged from $(4.12 \pm 0.30) \times 10^{-13}$ to $(13.2 \pm 1.17) \times 10^{-13}$ cm^3 $molecules^{-1}$ s^{-1}. These multiphase reaction rates correspond to

https://doi.org/10.5194/egusphere-2026-5464
Preprint. Discussion started: 29 September 2026

extended atmospheric lifetimes of 9.7 ± 3.3 to 31 ± 11 days, which translated into characteristic travel distances spanning 1.43×10^3 to 2.86×10^3 km and overall persistence (P_{OV}) values of 1.08×10^2 to 5.19×10^2 days in the environment.

Our findings revealed a significant phase-dependent kinetic inhibition; the determined k_{exp} values in the particle phase fall at least an order of magnitude below classical AOPWIN gas-phase estimates, highlighting that gas-phase models severely underestimate the actual atmospheric lifetime of BT-UVs. Furthermore, increasing RH from 25% to 50% increased k_{exp} by approximately 30% and shortened their lifetimes on aerosol particles. In contrast, the co-presence soluble Fe(II) yielded only a marginal increase in k_{exp} under the tested conditions. Regarding transformation pathways, multiphase $^{\bullet}OH$ oxidation proceeded predominantly via alkyl-group and phenyl-ring reactions. Importantly, among the 30 tentatively identified TPs in the OFR, 24 were successfully detected in authentic $PM_{2.5}$ samples from urban Shanghai, corroborating that these heterogeneous aging mechanisms actively occur in the real atmosphere.

While this study provides foundational kinetic data, several considerations still remain when extrapolating these findings to real atmospheric environments. Specifically, owing to the inherent limitations of the idealized core-shell particle system and the specific RH/Fe constraints employed here, the derived oxidation rate constants and lifetimes may not fully encompass the complexity of ambient aerosols. Real atmospheric aerosols exhibit immense diversity in chemical composition, viscosity, and morphology. Additionally, the presence of other reactive oxygen species (ROS) or light-absorbing organic matrices could further modulate their aging rates and transformation pathways. Therefore, future research considering complex aerosol matrices, phase states, and multi-oxidant conditions is warranted.

Despite these uncertainties, sufficient evidence presented here fundamentally advances our understanding of the atmospheric fate of particle-associated BT-UVs. Their extended chemical lifetimes (weeks) and calculated transport metrics directly demonstrate that BT-UVs possess long-range environmental transport potential comparable to that of established POPs governed by OECD criteria. Furthermore, the pervasive detection of oxygenated TPs with predicted enhanced ecotoxicity highlights that atmospheric transformation acts not merely as a sink, but as a secondary source of novel pollutants. Consequently, incorporating these multiphase kinetics and particulate TPs into global chemical transport models is essential to accurately assess their global distribution, deposition fluxes, and potential human inhalation exposure risks in the atmospheric environment.

Supplement

Detailed information is available in the Supplement.

Code and data availability

The data supporting this article have been included as part of the Supplement or are available by contacting the corresponding author (zhoulei@ecust.edu.cn).

https://doi.org/10.5194/egusphere-2026-5464
Preprint. Discussion started: 29 September 2026

Author contributions

Writing-original draft preparation, K, G; methodology, T, Z and L, Z; writing-review and editing X, W and G, X; funding acquisition and review, L, Z. All authors have read and agreed to the published version of the manuscript.

Competing interests

The authors declare that they have no conflict of interest.

Acknowledgements

This work gratefully acknowledges SCIEX for the high-performance mass spectrometry platform and related technical support.

Financial support

This work was financially supported by the National Natural Science Foundation of China (No. 22676060).

References

Antiñolo, M., Willis, M. D., Zhou, S., and Abbatt, J. P. D.: Connecting the oxidation of soot to its redox cycling abilities, Nature Communications, 6, 6812, 10.1038/ncomms7812, 2015.

Atkinson, R.: Kinetics and mechanisms of the gas-phase reactions of the hydroxyl radical with organic compounds under atmospheric conditions, Chemical Reviews, 86, 69-201, 10.1021/cr00071a004, 2002.

Awonaike, B., Lei, Y., Parajulee, A., and Wania, F.: Phase Partitioning, Transport and Sources of Benzotriazole Ultraviolet Stabilizers During a Runoff Event, Water Research X, 13, 100115, 10.1016/j.wroa.2021.100115, 2021.

Bai, L., Zhang, X., Li, J., Wang, Y., and Jiang, G.: Widening the Lens on Ultraviolet Absorbers: New Evidence from the Microenvironment of Agricultural Greenhouses and Workers' Risk Ranking Based on External Exposure and Internal Metabolic Processes, Environmental Science & Technology, 59, 10510-10521, 10.1021/acs.est.5c00738, 2025.

Birdsall, A. W., Andreoni, J. F., and Elrod, M. J.: Investigation of the Role of Bicyclic Peroxy Radicals in the Oxidation Mechanism of Toluene, The Journal of Physical Chemistry A, 114, 10655-10663, 10.1021/jp105467e, 2010.

Castilloux, A. D., Houde, M., Gendron, A., De Silva, A., Soubaneh, Y. D., and Lu, Z.: Distribution and Fate of Ultraviolet Absorbents and Industrial Antioxidants in the St. Lawrence River, Quebec, Canada, Environ Sci Technol, 56, 5009-5019, 10.1021/acs.est.1c07932, 2022.

CCTE, E.: Toxicity Estimation Software Tool (TEST), 10.23645/epacomptox.21379365.v3, 2022.

https://doi.org/10.5194/egusphere-2026-5464
Preprint. Discussion started: 29 September 2026

Chan, M. N., Zhang, H., Goldstein, A. H., and Wilson, K. R.: Role of Water and Phase in the Heterogeneous Oxidation of Solid and Aqueous Succinic Acid Aerosol by Hydroxyl Radicals, The Journal of Physical Chemistry C, 118, 28978-28992, 10.1021/jp5012022, 2014.

Chen, H., Hu, X., and Yin, D.: Benzotriazole ultraviolet stabilizers in the environment: A review of occurrence, partitioning and transformation, Science of The Total Environment, 954, 176362, https://doi.org/10.1016/j.scitotenv.2024.176362, 2024.

Cousins, I. T., Ng, C. A., Wang, Z., and Scheringer, M.: Why is high persistence alone a major cause of concern?, Environmental Science: Processes & Impacts, 21, 781-792, 10.1039/C8EM00515J, 2019.

Daumit, K. E., Carrasquillo, A. J., Sugrue, R. A., and Kroll, J. H.: Effects of Condensed-Phase Oxidants on Secondary Organic Aerosol Formation, The Journal of Physical Chemistry A, 120, 1386-1394, 10.1021/acs.jpca.5b06160, 2016.

Davidovcits, P., Kolb, C., Williams, L., Jayne, J., and Worsnop, D.: Mass Accommodation and Chemical Reactions at Gas−Liquid Interfaces, Chemical reviews, 106, 1323-1354, 10.1021/cr040366k, 2006.

EPA, U.: Methods for Derivation of Inhalation Reference Concentrations and Application of Inhalation Dosimetry, 1994.

European Chemicals Agency: https://echa.europa.eu, last access: 1 September 2026.

Fuks, N. A. and Sutugin, A. G.: Highly dispersed aerosols, Ann Arbor Science Publishers, Ann Arbor1970.

Han, L., Zhao, P., and Zetzsch, C.: Heterogeneous Reaction of OH Radicals with Terbuthylazine on Self-synthesized Silica Particles in an Aerosol Smog Chamber at Different Temperatures, Aerosol Science and Engineering, 5, 451-459, 10.1007/s41810-021-00114-5, 2021.

He, K., Yang, F., Ma, Y., Zhang, Q., Yao, X., Chan, C. K., Cadle, S., Chan, T., and Mulawa, P.: The characteristics of $PM_{2.5}$ in Beijing, China, Atmospheric Environment, 35, 4959-4970, https://doi.org/10.1016/S1352-2310(01)00301-6, 2001.

Huang, Y. Y., Wang, X., Xie, L., De Silva, A., Brinovcar, C., Peng, H., Wania, F., and Abbatt, J.: O_3 and OH Multiphase Oxidation of Benzotriazole Ultraviolet Stabilizer UV-328, Environmental Science & Technology, 10.1021/acs.est.6c01932, 2026.

Jacobson, M. Z.: Fundamentals of Atmospheric Modeling, 2, Cambridge University Press, Cambridge, DOI: 10.1017/CBO9781139165389, 2005.

Laversin, H., El Masri, A., Al Rashidi, M., Roth, E., and Chakir, A.: Kinetic of the gas-phase reactions of OH radicals and Cl atoms with diethyl ethylphosphonate and triethyl phosphate, Atmospheric Environment, 126, 250-257, https://doi.org/10.1016/j.atmosenv.2015.11.057, 2016.

Lawrence, M. G., Jöckel, P., and von Kuhlmann, R.: What does the global mean OH concentration tell us?, Atmos. Chem. Phys., 1, 37-49, 10.5194/acp-1-37-2001, 2001.

Li, Q., Wyatt, A., and Kamens, R. M.: Oxidant generation and toxicity enhancement of aged-diesel exhaust, Atmospheric Environment, 43, 1037-1042, https://doi.org/10.1016/j.atmosenv.2008.11.018, 2009.

Li, R., Palm, B. B., Ortega, A. M., Hlywiak, J., Hu, W., Peng, Z., Day, D. A., Knote, C., Brune, W. H., de Gouw, J. A., and Jimenez, J. L.: Modeling the Radical Chemistry in an Oxidation Flow Reactor: Radical Formation and Recycling, Sensitivities, and the OH Exposure Estimation Equation, The Journal of Physical Chemistry A, 119, 4418-4432,

https://doi.org/10.5194/egusphere-2026-5464
Preprint. Discussion started: 29 September 2026

10.1021/jp509534k, 2015.

Ling, T., Fang, Y., Zong, L., Tang, Z., Fan, K., Chen, D., Jin, P., and Guan, M.: Review of Environmental Occurrence and Toxicity of Benzotriazole Ultraviolet Stabilizers, Environment & Health, 3, 1438-1455, 10.1021/envhealth.5c00139, 2025.

Liu, Q., Liggio, J., Li, K., Lee, P., and Li, S.-M.: Understanding the Impact of Relative Humidity and Coexisting Soluble Iron on the OH-Initiated Heterogeneous Oxidation of Organophosphate Flame Retardants, Environmental Science & Technology, 53, 6794-6803, 10.1021/acs.est.9b01758, 2019a.

Liu, Q., Liggio, J., Wentzell, J., Lee, P., Li, K., and Li, S.-M.: Atmospheric OH Oxidation Chemistry of Particulate Liquid Crystal Monomers: An Emerging Persistent Organic Pollutant in Air, Environmental Science & Technology Letters, 7, 646-652, 10.1021/acs.estlett.0c00447, 2020.

Liu, Q., Liggio, J., Wu, D., Saini, A., Halappanavar, S., Wentzell, J. J. B., Harner, T., Li, K., Lee, P., and Li, S.-M.: Experimental Study of OH-Initiated Heterogeneous Oxidation of Organophosphate Flame Retardants: Kinetics, Mechanism, and Toxicity, Environmental Science & Technology, 53, 14398-14408, 10.1021/acs.est.9b05327, 2019b.

Liu, Q., Li, L., Zhang, X., Saini, A., Li, W., Hung, H., Hao, C., Li, K., Lee, P., Wentzell, J. J. B., Huo, C., Li, S.-M., Harner, T., and Liggio, J.: Uncovering global-scale risks from commercial chemicals in air, Nature, 600, 456-461, 10.1038/s41586-021-04134-6, 2021.

Liu, Y., Liggio, J., Harner, T., Jantunen, L., Shoeib, M., and Li, S.-M.: Heterogeneous OH Initiated Oxidation: A Possible Explanation for the Persistence of Organophosphate Flame Retardants in Air, Environmental Science & Technology, 48, 1041-1048, 10.1021/es404515k, 2014.

Lu, Z., Smyth, S. A., Peart, T. E., and De Silva, A. O.: Occurrence and fate of substituted diphenylamine antioxidants and benzotriazole UV stabilizers in various Canadian wastewater treatment processes, Water Research, 124, 158-166, https://doi.org/10.1016/j.watres.2017.07.055, 2017.

Maceira, A., Borrull, F., and Marcé, R. M.: Occurrence of plastic additives in outdoor air particulate matters from two industrial parks of Tarragona, Spain: Human inhalation intake risk assessment, J Hazard Mater, 373, 649-659, 10.1016/j.jhazmat.2019.04.014, 2019.

Mackay, D., Di Guardo, A., Paterson, S., and Cowan, C. E.: Evaluating the environmental fate of a variety of types of chemicals using the EQC model, Environmental Toxicology and Chemistry, 15, 1627-1637, 10.1002/etc.5620150929, 1996.

Meylan, W. M. and Howard, P. H.: Computer estimation of the Atmospheric gas-phase reaction rate of organic compounds with hydroxyl radicals and ozone, Chemosphere, 26, 2293-2299, https://doi.org/10.1016/0045-6535(93)90355-9, 1993.

Miyamoto, S., Martinez, G. R., Medeiros, M. H. G., and Di Mascio, P.: Singlet Molecular Oxygen Generated from Lipid Hydroperoxides by the Russell Mechanism: Studies Using 18O-Labeled Linoleic Acid Hydroperoxide and Monomol Light Emission Measurements, Journal of the American Chemical Society, 125, 6172-6179, 10.1021/ja029115o, 2003.

Nakata, H., Murata, S., and Filatreau, J.: Occurrence and Concentrations of Benzotriazole UV Stabilizers in Marine Organisms and Sediments from the Ariake Sea, Japan, Environmental Science & Technology, 43, 6920-6926, 10.1021/es900939j, 2009.

https://doi.org/10.5194/egusphere-2026-5464
Preprint. Discussion started: 29 September 2026

Organisation for Economic Co-operation and Development (OECD): https://hpvchemicals.oecd.org/ui/ChemGroup.aspx, last access: 1 September 2026.

Parajulee, A., Lei, Y. D., Kananathalingam, A., Mitchell, C. P. J., and Wania, F.: Investigating the Sources and Transport of Benzotriazole UV Stabilizers during Rainfall and Snowmelt across an Urbanization Gradient, Environmental Science & Technology, 52, 2595-2602, 10.1021/acs.est.8b00552, 2018.

Peng, Z. and Jimenez, J. L.: Radical chemistry in oxidation flow reactors for atmospheric chemistry research, Chemical Society Reviews, 49, 2570-2616, 10.1039/C9CS00766K, 2020.

Peng, Z., Palm, B. B., Day, D. A., Talukdar, R. K., Hu, W., Lambe, A. T., Brune, W. H., and Jimenez, J. L.: Model Evaluation of New Techniques for Maintaining High-NO Conditions in Oxidation Flow Reactors for the Study of OH-Initiated Atmospheric Chemistry, ACS Earth and Space Chemistry, 2, 72-86, 10.1021/acsearthspacechem.7b00070, 2018.

Perala-Dewey, J. and Hageman, K. J.: Atmospheric Transport of Semivolatile Organic Contaminants across an Urban-Alpine Boundary, Environmental Science & Technology, 58, 18313-18323, 10.1021/acs.est.4c03373, 2024.

Pflieger, M., Monod, A., and Wortham, H.: Heterogeneous Oxidation of Terbuthylazine by “Dark” OH Radicals under Simulated Atmospheric Conditions in a Flow Tube, Environmental Science & Technology, 47, 6239-6246, 10.1021/es3052203, 2013.

Reid, J. P., Dennis-Smither, B. J., Kwamena, N.-O. A., Miles, R. E. H., Hanford, K. L., and Homer, C. J.: The morphology of aerosol particles consisting of hydrophobic and hydrophilic phases: hydrocarbons, alcohols and fatty acids as the hydrophobic component, Physical Chemistry Chemical Physics, 13, 15559-15572, 10.1039/C1CP21510H, 2011.

Russell, G. A.: Deuterium-isotope Effects in the Autoxidation of Aralkyl Hydrocarbons. Mechanism of the Interaction of PEroxy Radicals1, Journal of the American Chemical Society, 79, 3871-3877, 10.1021/ja01571a068, 1957.

Shunthirasingham, C., Zhan, F., Rabu, M., Oh, J., Li, Y., Lei, Y. D., Hung, H., Lu, Z., Gobas, F. A. P. C., Moradi, M., and Wania, F.: Scant Evidence for Long-Range Atmospheric Transport of Particle-Bound Benzotriazole Ultraviolet Stabilizers, Environmental Science & Technology, 59, 2641-2650, 10.1021/acs.est.4c11623, 2025.

Stockholm Convention on Persistent Organic Pollutants (POPs): https://chm.pops.int, last access: 1 September 2026.

Slade, J. H. and Knopf, D. A.: Multiphase OH oxidation kinetics of organic aerosol: The role of particle phase state and relative humidity, Geophysical Research Letters, 41, 5297-5306, https://doi.org/10.1002/2014GL060582, 2014.

Smith, J. D., Kroll, J. H., Cappa, C. D., Che, D. L., Liu, C. L., Ahmed, M., Leone, S. R., Worsnop, D. R., and Wilson, K. R.: The heterogeneous reaction of hydroxyl radicals with sub-micron squalane particles: a model system for understanding the oxidative aging of ambient aerosols, Atmos. Chem. Phys., 9, 3209-3222, 10.5194/acp-9-3209-2009, 2009.

Song, M., Marcolli, C., Krieger, U. K., Lienhard, D. M., and Peter, T.: Morphologies of mixed organic/inorganic/aqueous aerosol droplets, Faraday Discussions, 165, 289-316, 10.1039/C3FD00049D, 2013.

Van Leeuwen, K. V. L.: Technical guidance document on risk assessment in support of commission directive 93/67/EEC on risk assessment for new notified substances and commission regulation (EC) No1488/94 on risk assessment for existing substances Part II, Euro. Commun., 1-337, 1996.

https://doi.org/10.5194/egusphere-2026-5464
Preprint. Discussion started: 29 September 2026

Wang, X., Wang, W., Wingen, L. M., Perraud, V., and Finlayson-Pitts, B. J.: Top–down versus bottom–up oxidation of a neonicotinoid pesticide by OH radicals, Proceedings of the National Academy of Sciences, 121, e2312930121, 10.1073/pnas.2312930121, 2024.

Wegmann, F., Cavin, L., MacLeod, M., Scheringer, M., and Hungerbühler, K.: The OECD software tool for screening chemicals for persistence and long-range transport potential, Environmental Modelling & Software, 24, 228-237, https://doi.org/10.1016/j.envsoft.2008.06.014, 2009.

Worsnop, D. R., Morris, J. W., Shi, Q., Davidovits, P., and Kolb, C. E.: A chemical kinetic model for reactive transformations of aerosol particles, Geophysical Research Letters, 29, 57-51-57-54, https://doi.org/10.1029/2002GL015542, 2002.

Yang, Y., Zhang, Q., Li, K., Liu, Y., Guo, F., and Xia, X.: LC–HRMS Screening, Risk Assessment, and Source Tracing of Neonicotinoid Insecticides and Their Transformation Products in China's Coastal Urban Rivers, Environmental Science & Technology, 60, 8749-8761, 10.1021/acs.est.5c18084, 2026.

Zhang, S., Wang, Z., Chen, J., Xie, Q., Zhu, M., and Han, W.: Tissue-Specific Accumulation, Biotransformation, and Physiologically Based Toxicokinetic Modeling of Benzotriazole Ultraviolet Stabilizers in Zebrafish (Danio rerio), Environmental Science & Technology, 55, 11874-11884, 10.1021/acs.est.1c02861, 2021.

Zhang, Z., Ren, N., Li, Y.-F., Kunisue, T., Gao, D., and Kannan, K.: Determination of Benzotriazole and Benzophenone UV Filters in Sediment and Sewage Sludge, Environmental Science & Technology, 45, 3909-3916, 10.1021/es2004057, 2011.

Zhao, Y., Bai, L., Wang, X., Huo, M., Gao, W., Jiang, L., Jin, J., Wang, Y., and Cao, D.: Exposure Assessment of Benzotriazole Ultraviolet Absorbers in Plastic Sports Field Dust and Indoor Dust: Are Plastic Sports Fields High Exposure Scenarios?, Environmental Science & Technology, 58, 17419-17428, 10.1021/acs.est.4c03930, 2024.

Zhou, S., Shiraiwa, M., McWhinney, R. D., Pöschl, U., and Abbatt, J. P. D.: Kinetic limitations in gas-particle reactions arising from slow diffusion in secondary organic aerosol, Faraday Discussions, 165, 391-406, 10.1039/C3FD00030C, 2013.